Journal of
Nanoscience and Nanotechnology
Vol. 12, 1–10, 2012

Surface Modification and Bioactivity of Anodic Ti6Al4V Alloy

Khairul Arifah Saharudin[1], Srimala Sreekantan[1,*], Siti Nor Qurratu Aini Abd Aziz[1], Roshasnorlyza Hazan[1], Chin Wei Lai[1], Rabiatul Basria S. M. N. Mydin[2], and Ishak Mat[2]

[1]*School of Materials and Mineral Resources Engineering, Universiti Sains Malaysia, Engineering Campus, 14300 Nibong Tebal, Seberang Perai Selatan, Pulau Pinang, Malaysia*
[2]*Advance Medical and Dental Institute, Eureka Complex, Universiti Sains Malaysia, 11800 Pulau Pinang, Malaysia*

The present study deals with surface modification of Ti6Al4V alloy via anodization technique. The morphology, structure, adhesion and bioactivity of Ti6Al4V alloy after anodization process were investigated in detail. The influence of fluoride content and direct circuit (DC) applied voltage during anodization of Ti6Al4V alloy in a bath with electrolytes composed of ethylene glycol (EG) and ammonium fluoride (NH_4F) were considered. It was found that the average pore sizes and length of nanoporous or nanotubes were increasing with the fluoride content and applied voltage. A minimum of 3 wt% of NH_4F is required to grow a self-organized nanotube arrays. As the fluoride content was increased to 5 wt%, TiO_2 nanotubes with average diameter of 110 nm and 3.4 μm lengths were successfully synthesized. It is noteworthy to point out that the rate of the nanotube formation was increasing up to 9 μm thick bioactive TiO_2 nanotubes layer as anodization time was increased to 3 h. Based on the results obtained, the PA6 cells cultured on anodic Ti6Al4V alloy showed highest level of cell viability and greater cell adhesion compared to the flat Ti6Al4V foil substrate. In fact, highly ordered nanotubes structure on Ti6Al4V alloy can provide beneficial effects for PA6 cells in attachment and proliferation.

Keywords: Ti6Al4V Alloy, Anodization, Cell Proliferation.

RESEARCH ARTICLE

1. INTRODUCTION

Titanium (Ti) or Ti alloys implant exhibits good bioactivity, good mechanical properties and excellent corrosion resistance in application as an osseointegrative implant materials.[1–3] In order to improve the bioactivity of Ti6Al4V alloy, surface modification by creating porous nanotubular structures has been considered as one of the ways to improve its performance since the topography is changed as well as increased active surface area.[4–6] Modifications of Ti6Al4V surfaces, for example chemical treatment in alkali solution and anodic oxidation leads to formation of active TiO_2 coatings.[4, 8–9] Furthermore nanostructured coating on Ti alloy improves osteoblast adhesion, proliferation and mineralization.[10] In fact, different surface treatments will have dissimilar effects on the bioactivity of implants surface.[11, 12]

Surface treatment via anodization is combined with thermal treatment to obtain high biocompatibility or stabilize the surface layer. The thermal treatment influence some chemical changes, structure and morphology changes to the surface layer. The TiO_2 nanotubes layer was annealed at a temperature up to 600 °C to form stable and more reactive layer on the surface.[12] Based on previous studies, Nishiguchi et al. and Kim et al. have been reported that the anodic oxidations with the thermal treatment to 500–600 °C for 1–2 h have a positive effect to bioactivity.[13, 14] It is a well known fact that TiO_2 nanotubes could be systematically thermal treated to control the transformation of as-anodized amorphous structure to crystalline anatase and rutile phase structure. Therefore, optimization of the crystallinity of TiO_2 nanotubes is an important task in order to enhance the bioactivity.

Over the past few years, many studies have been reported on the anodization of pure Ti and mechanisms of film formation have been well enough elucidated.[4–7] TiO_2 nanotubes have shown a good bioactivity in simulated body fluids and cell culture.[13–15] Based on this progress, anodization of Ti alloys to fabricate TiO_2 nanotubes have been attracted much attention recently. Tsuchiya et al. has

*Author to whom correspondence should be addressed.

been reported on the formation of nanostructured oxide films on TiAl and Ti–Ta alloys since 2007.[16, 17] Later, Saji et al. has been discussed the formation of nanotubular oxide layers on Ti–35Nb–5Ta–7Zr alloy in 2009.[18] In fact, an earlier report by Ghicov et al. regarding to the anodization of Ti45Nb alloy to grow Ti–Nb–O nanotubes, which show enhanced thermal stability in comparison with that of TiO_2 nanotubes on pure Ti.[19] In addition, Auckland et al. has been claimed that development of nanostructured oxide films on Ti–Nb and Ti–Ta that has lower surface resistance and improved chemical stability than pure Ti for proton exchange membrane (PEM) fuel cells.[20] Considering the great advantages (better corrosion resistance, higher wear resistance and enhanced tissue response) of Ti6Al4V alloy for clinical applications,[10, 21] oxide nanotubes grown on Ti6Al4V alloys are expected to have a bright future.

The effects of surface topography on cell adhesion have been extensively studied over the last decade, but no consensus has been reached. Several authors have reported an association between increased implant surface roughness (as a result of specific texturization techniques) and improved cell adhesion and proliferation findings.[16, 22–24] However, many studies have been proved that this technique increased the surface roughness and it was not a determinant factor for initial cell response.[25–26] Finally, an *in vitro* study has suggested that osteoblasts show a preference for surfaces with a high degree of microroughness (mean roughness of approximately 0.5 μm).[28] In the present study, developments of self organized nanotube arrays on Ti6Al4V alloy with optimize fluoride content, applied voltage and anodization time were investigated. The ultimate aim of the study was optimized the nanotube layer thickness, morphology and crystal structure to assess the proliferation of PA6 mouse bone marrow stromal cell cultured on these surfaces. The assessment was carried out using quantitative analysis of cell proliferation.

RESEARCH ARTICLE

2. EXPERIMENTAL PROCEDURE

2.1. TiO_2 Nanotubes Formation

Ti6Al4V alloys supplied by Straits Orthopaedics (Mfg) Sdn. Bhd. were used as substrates for the anodic growth of TiO_2 nanotube layers. The alloy samples with a size of $0.5 \times 0.5 \times 5$ cm^3 were ultrasonically cleaned for 30 minutes in a mixture solution of 1 M HNO_3 and 0.45 M NH_4F. After cleaning, the samples were rinsed with deionized water and air dried. For anodization an electrochemical cell with 2 electrode configuration was used. Platinum electrode served as cathode and Ti6Al4V served as anode. Electrochemical experiments were carried out using a Keithley 2611 A system sourcemeter. The anodization has been made at different fluoride amount of 1, 3, 4 and 5 wt% of NH_4F and direct current voltage varied from 10 to 60 V. Nanotubes formation was achieved at potential 60 V and time ranging from 20 seconds to 6 hour. After anodization the samples were ultrasonically cleaned in acetone for 1 minute, rinsed with deionized water and dried in nitrogen stream. The as-anodized samples were heat treated by annealing at temperature ranging from 400 to 600 °C. For morphological characterization of samples, field emission scanning electron microscope (FESEM-Zeiss, Supra 35VP) was used and the crystal structure of the TiO_2 nanotubes was studied by X-ray diffraction (Phillip model PW 1729). The surface roughness of TiO_2 nanotubes samples were characterized using SPA 300 HV Scanning Probe Microscope.

2.2. PAC (Bone Marrow Stromal Cell Lines) Culture

Two samples; Ti6Al4V alloy and TiO_2 nanotubes formed on Ti6Al4V alloy were cut into 5×3 mm in dimension. TiO_2 nanotubes samples were annealed at 400 °C to obtain anatase phase. Each of samples was placed in separate bottle. The samples were then autoclaved at 120 °C for 20 minutes. All the samples were put in the 96 well plates. 200 μl α-MEM Gibco medium (10% Fetal Bovine Serum (Gibco) + 1% Penicilin Steptomicin + Gentamicin + Amphoterin) was put in each well. The cells are seeded at concentration of 1×10^5 cells/well. The prepared samples were then incubated for 1, 3 and 7 days in 5% CO_2 + 95% air at 37 °C. Then the cell morphology was observed and the viable attached cells counted as a function of incubation time.

2.3. MTS Proliferation Assay

The density of viable cells was estimated. MTS assays (promega) are colorimetric assays for measuring the activity of enzymes that close dyed to formazan dyes, giving a purple color. After the selected incubation periods, the samples were washed 3 times by PBS and transferred to a new 96-well polystyrene culture plate. A 40 μl quantity of MTS dye agent added to each well followed by 200 μl complete α-MEM Gibco medium. After 3 hour of incubation in a 5% CO_2 incubator, all media were put in each well of 96-well polystyrene culture plate. Finally the absorbance of each solution was measured at a wavelength of 490 nm by ELISA plate reader.

3. RESULTS AND DISCUSSION

3.1. Effect of NH_4F Content

The variations on surface morphology of the anodic Ti6Al4V alloy with different NH_4F concentrations during the anodization at 60 V for 1 hour are presented in Figures 1(a)–(d). Anodization of Ti6Al4V alloy in electrolyte containing 1 wt% of NH_4F formed an irregular nanoporous structure with 2.3 μm (Fig. 1(a)) on the surface Ti6Al4V alloy. It could be observed that parts of

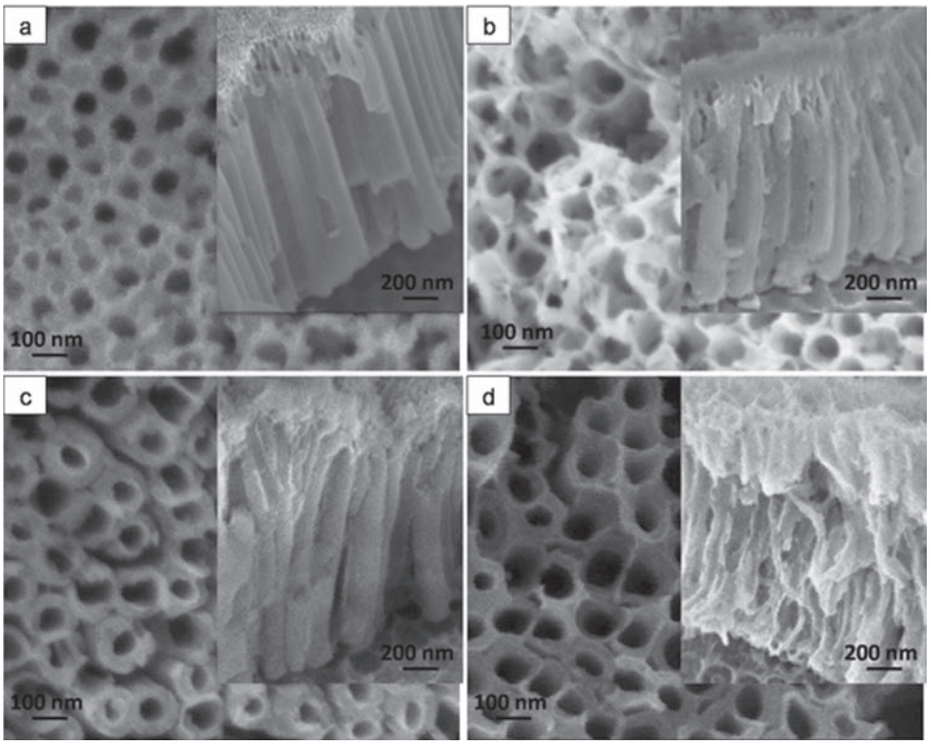

Fig. 1. FESEM images of Ti6Al4V alloys anodized in EG + 1–5 wt% NH_4F at 60 V for 1 hour. (a) 1 wt%, (b) 3 wt%, (c) 4 wt%, (d) 5 wt%.

the anodic oxide layer were covered with small pits and larger pores. The reason mainly attributed to the different in the degree of localized dissolution of the oxide layer. Figure 1(b) shows the Ti6Al4V alloys anodized in EG containing 3 wt% NH_4F. It was noticed that pits and pores have been started to convert into sponge like structure. The inset shows the thickness of sponge like structures of about 2.3 μm. Besides, it could also be noticed that the entire Ti6Al4V alloy surface was not uniformly covered with nanoporous structure.

For 4 wt% and 5 wt% NH_4F, self organized TiO_2 nanotubes array was formed (Figs. 1(c) and (d)). The average diameter of the nanotubes is approximately 81 and 110 nm for 4 wt% and for 5 wt%, respectively, while the nanotubes length is 3.4 μm for both samples. Generally, the pores or the nanotube diameter are found to be larger with increasing fluoride content in the electrolyte. It is worth to note that the growth of TiO_2 nanotubes depends on the oxide growth rate and the chemical dissolution of the oxide by fluoride ion. Excess fluoride ion increases the electrical field intensity at the bottom of the pore thus drives further oxidation, and field assisted dissolution where Ti ions come out of the metal and dissolve in solution. This indicates that the chemical dissolution of anodic oxide later is induced by fluoride ion.[29–32]

The corresponding XRD patterns of the Ti alloy sheet as a function of fluoride content are shown in Figure 2. After annealing at 400 °C, the diffraction peak appears at 2θ of 25° representing (101) plane of anatase TiO_2. In addition, diffraction pattern of α-Ti at $2\theta = 35.18°$, 40.26°, 53.08° and 63.19° corresponding to the (100), (101), (102), (110) plane and β-Ti peak at 38.75° corresponding at (002) plane were detected. These peaks are originated from the substrate of the Ti alloy. It is worth to note that the peak intensity of α and β Ti decreased as the content of fluoride increased. This is likely due to larger thickness of the oxide layer formed on the Ti6Al4V alloy.

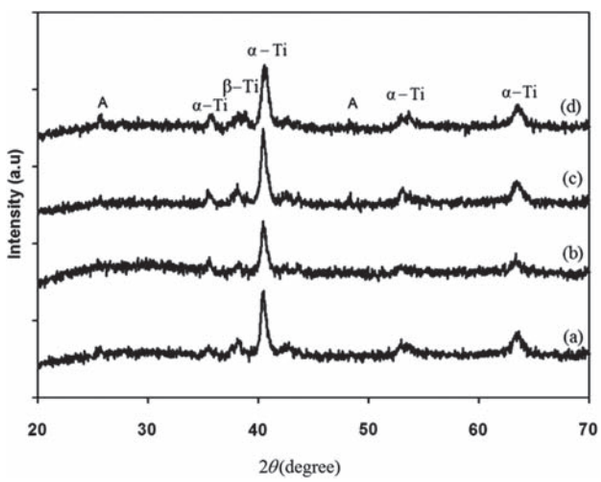

Fig. 2. XRD pattern of Ti6Al4V alloys anodized in EG + 1–5 wt% NH_4F at 60 V for 1 hour and annealed at 400 °C for 4 hours in argon atmosphere. (a) 1 wt%, (b) 3 wt%, (c) 4 wt%, and (d) 5 wt% weight of NH_4F. A = Anatase, α-Ti = alpha Ti and β-Ti = Beta Ti.

RESEARCH ARTICLE

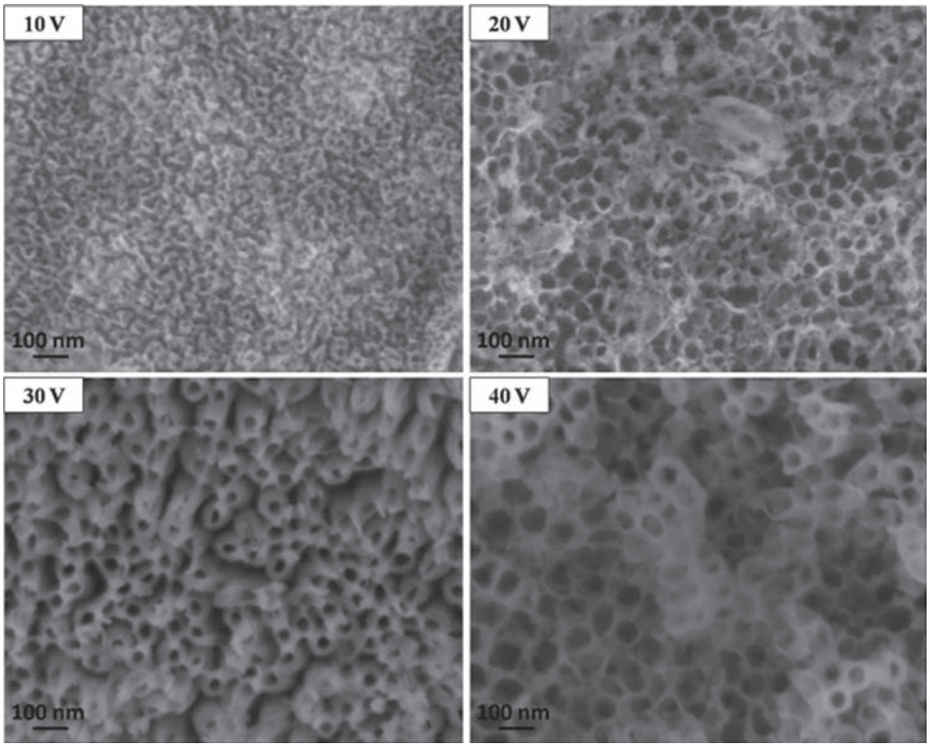

Fig. 3. FESEM images of Ti6Al4V alloys anodized in EG + 5 wt% NH_4F at voltage varied from 10–40 V for 1 hour.

3.2. Effect of DC Applied Voltage

The influence of DC applied voltage on the morphology of oxide layers prepared by anodization of Ti alloys in an electrolyte bath composed of EG and 5 wt% of NH_4F as exhibited in Figure 3. The effect of applied voltage was observed in the range of 10–60 V. At 10 V, small pits are observed on the surface of the oxide layer. At this stage the dissolution of Ti had just occurred. As the voltage increased to 20 V, the pits nucleate to form large porous structure. However, not all the surface is covered with porous TiO_2. There are still areas covered with compact oxide layer. This is due to the insufficient voltage to induce complete dissolution and breakdown of barrier layers to dissolve the oxide into tubes.[21, 33]

When applied voltage was increased to 30 V up to 60 V, self organized nanotube arrays are formed. However the lengths of the nanotubes in certain area are relatively low as compared to others. This finding is different compared to few authors who claimed the existence of two kinds of the nanostructure on the surface of the Ti6Al4V alloy. One was self organized nanotube arrays and the other was irregular nanoporous structure. According to few authors,[34, 22] the self organized nanotubes arrays are proven to be grown on the α phase region and nanoporous structure on β phase region. The α phase are enriched with Al whereas β phase region enriched with V. Because of the different chemistries of these phases, the formation of the nanotubular oxide layer is not uniform as β phases get etched preferentially by the electrolyte. Different results were obtained in this work probably due to different electrolyte used. Most of the aforementioned studies utilize aqueous solution which subjected high chemical dissolution rate. In here the use of EG with pH 6.5 could avoid the significant attack on β phase and produce homogeneous microstructure. However, the length of the nanotubes are different within the α and β phase region, being short at β phase region as the solubility of V is faster than the Al.

3.3. Effect of Anodization Time

Figure 4 shows the different surfaces that were obtained by anodizing the Ti6Al4V alloy for varying durations at 60 V in EG electrolyte containing 5 wt% NH_4F. In the early stage of anodization (20 seconds), compact oxide layers are formed on the surface of the of Ti6Al4V alloy due to the interaction within O^{2-} and OH^-. After 1 minute the oxide layer has been etched in certain area, thus forming irregular pits due to localized dissolution. After 5 minutes of anodization, the pits are converted to larger pores with most of the areas are still covered with oxide layer. At 10 minutes, a breakdown of the compact TiO_2 layer occurred on the surface, after which a porous TiO_2 layer gradually grow and the TiO_2 nanotubes with average length of 4 μm was obtained. After 15 minutes, the surface is completely filled with self organized nanotubes arrays. For 30 minutes, the morphology become stable and gradually grows up to 9 μm after 6 hour anodization. The overall

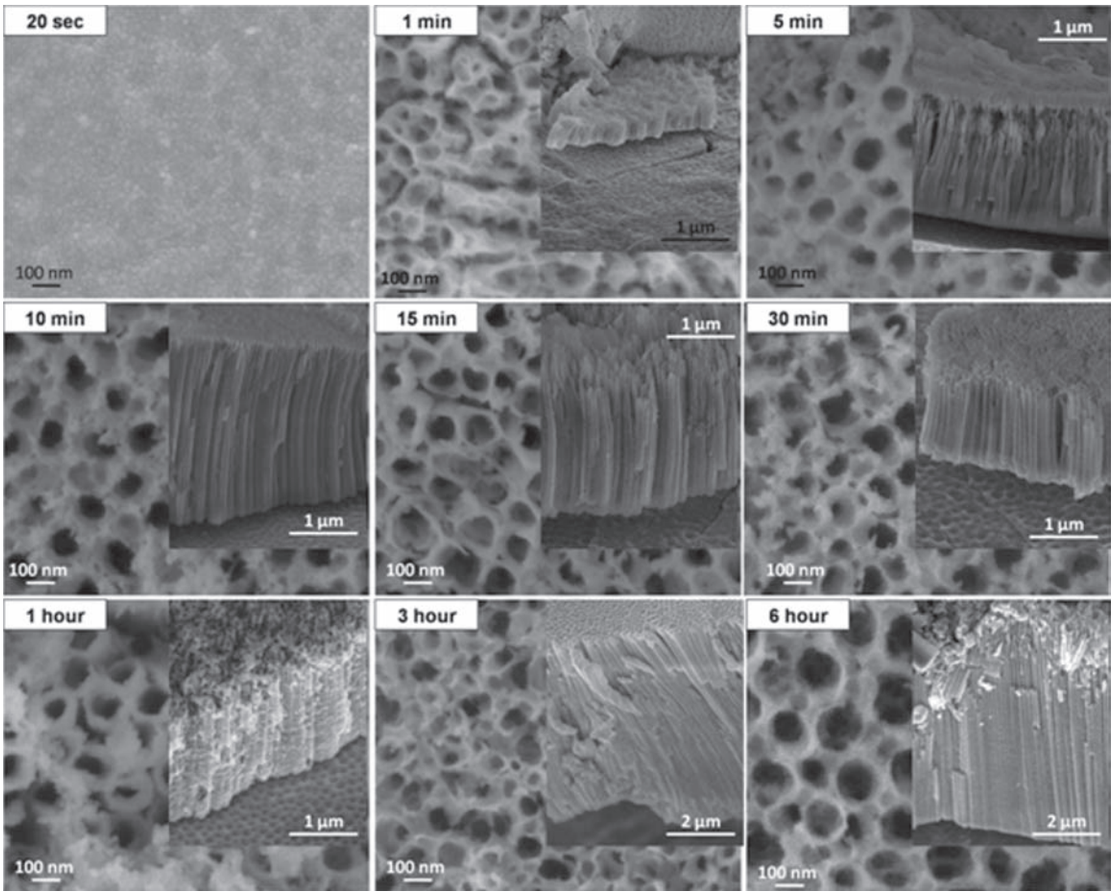

Fig. 4. FESEM images of TiO_2 nanotubes formed at 60 V in EG + 5 wt% NH_4F at various anodization time.

formation of the nanotubes on Ti6Al4V alloy is similar to the Ti–8Mn reported by Mohapatra et al.[35] The diameter and length of TiO_2 nanotubes formed are presented in Table I.

The graph in Figure 5 shows the current density as a function of anodization time. Such plot is important to explain the mechanism of TiO_2 nanotube formation. In the initial stage of anodization (noted as region I), an abrupt decrease of current was observed due to the formation of compact oxide film. According to Zhao et al.[36] this initial stage is known as passivation process of Ti as illustrated by Eq. (1).

$$Ti^{4+} + 2H_2O \rightarrow TiO_2 + 4H^+ \quad (1)$$

In second stage (noted as region II) occur due to the pronounced dissolution at the pore bottoms that takes place

Table I. Diameter and length of TiO_2 nanotubes formed at various anodization time.

Time (minutes)	Tube diameter (nm)	Tube length (μm)	Morphology
20 sec	–	–	Compact structure
1	–	0.5	Pits formation
5	64	2.4	Porous structure
10	70	4.0	Nanotubes
15	75	4.0	Nanotubes
30	100	2.8	Nanotubes
1 hour	110	3.4	Nanotubes
3 hour	110	9.0	Nanotubes
6 hours	150	9.0	Nanotubes

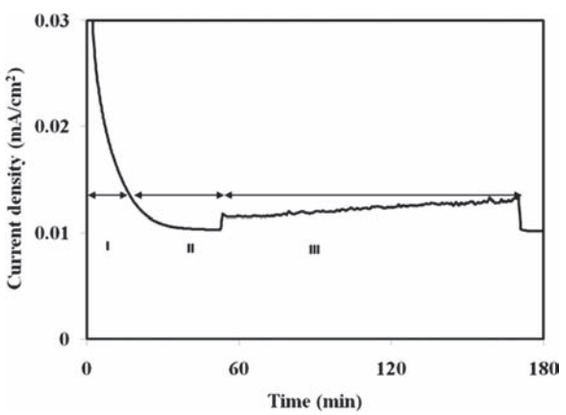

Fig. 5. Current time plot of Ti6Al4V anodization at 60 V in EG + 5 wt% NH_4F.

RESEARCH ARTICLE

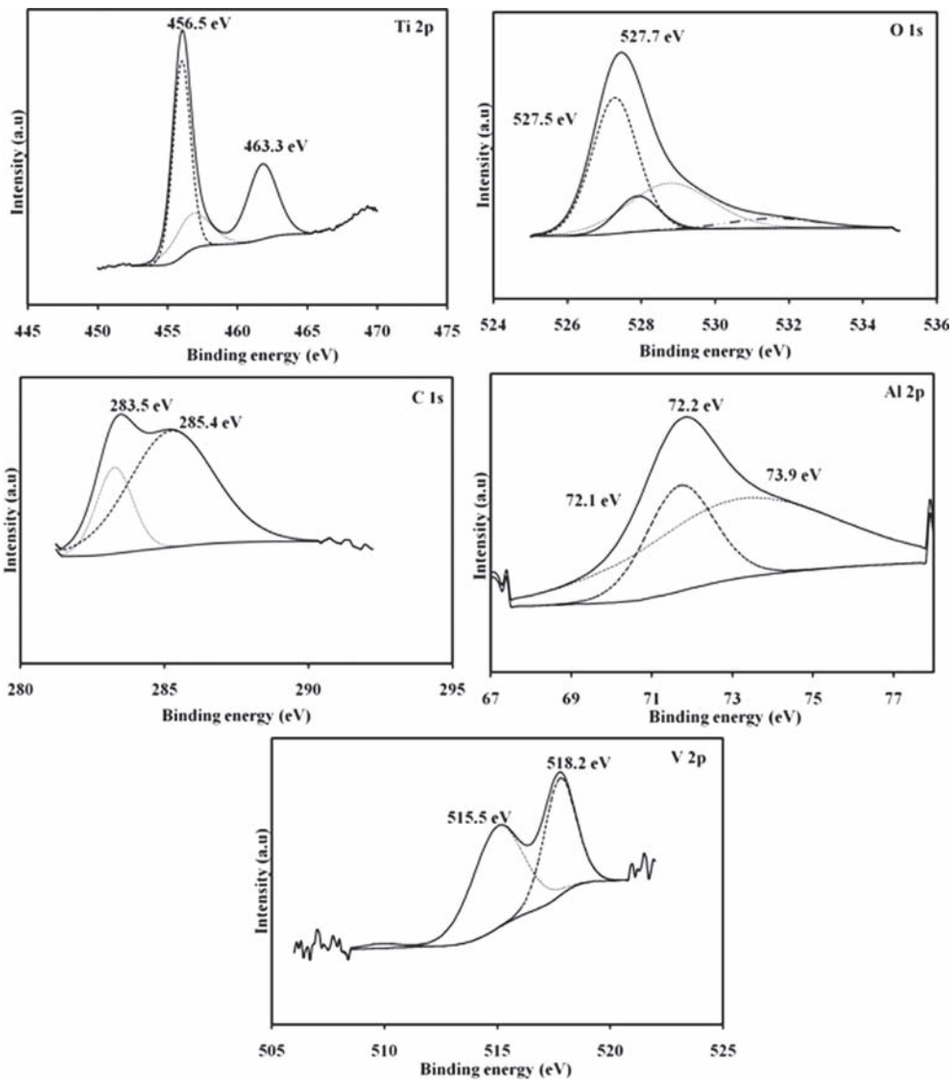

Fig. 6. XPS high-resolution spectrum of the anodic Ti6Al4V alloy surface: (a) Ti 2p, (b) O 1s, (c) C 1s, (d) Al 2p and (e) V 2p.

which makes them significantly deeper. This chemical dissolution reduces the thickness of the oxide barrier layer at the bottom of the pits and allows the electrochemical etching process to continue. The oxide layer at the bottom of the pits is relatively thin; and the thin layer, in turn, increases the electric field intensity, resulting in further pore growth.

In third stage (noted as region III), a constant equilibrium is maintained with the increasing anodizing time while current density is slightly reduced due to the changes of the pores depth of pits. The thickness increases until a steady-state situation is established.

3.4. Chemical Composition

The chemical composition present at the surface of Ti6Al4V nanotube subjected to annealing at 400 °C for 4 hours under Argon atmosphere was investigate using

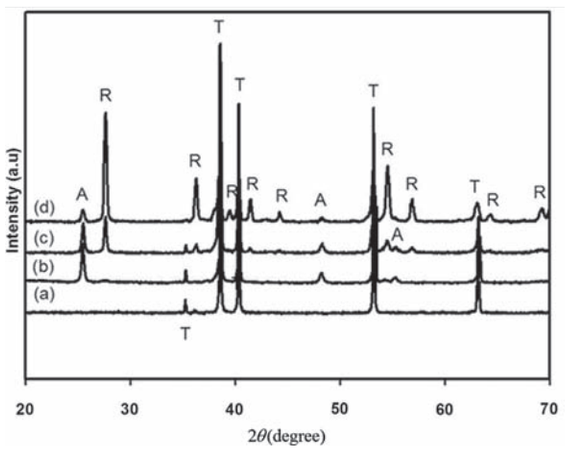

Fig. 7. XRD patterns of TiO_2 nanotubes formed at 60 V in EG+5 wt% NH_4F for 1 hour. (a) As-anodized, and annealed at (b) 400 °C, (c) 500 °C, (d) 600 °C.

RESEARCH ARTICLE

XPS analysis, and the result is shown in Figure 6. Based on the result, the binding energies of $Ti2p_{3/2}$ and $Ti2p_{1/2}$ were found at 456.5 eV and 463.3 eV, respectively. This is likely due to the presence of Ti^{4+} oxidation state.[37, 38] The Ti^{4+} ions reacted with O^{2-} ions during anodization, and consequently formed TiO_2. This was confirmed by the presence of Ti—O (527.5–527.7 eV) in O1s. Besides, the presence of OH^- ions and absorbed H_2O was detected at 528.9 eV and 531.9 eV. The C 1s spectra for TiO_2 made in ethylene glycol and glycerol were similar and revealed two peaks at 283.5 and 285.4 eV as well as an additional shoulder at 286.5 eV (Fig. 6(b)). The strong peak positioned at 283.5 eV is usually assigned to adventitious elemental carbon, which cannot be eliminated. This peak also existed in the case of the pure TiO_2 sample[39, 40] and it was close to the position of graphitic sp^2-hybridized carbon

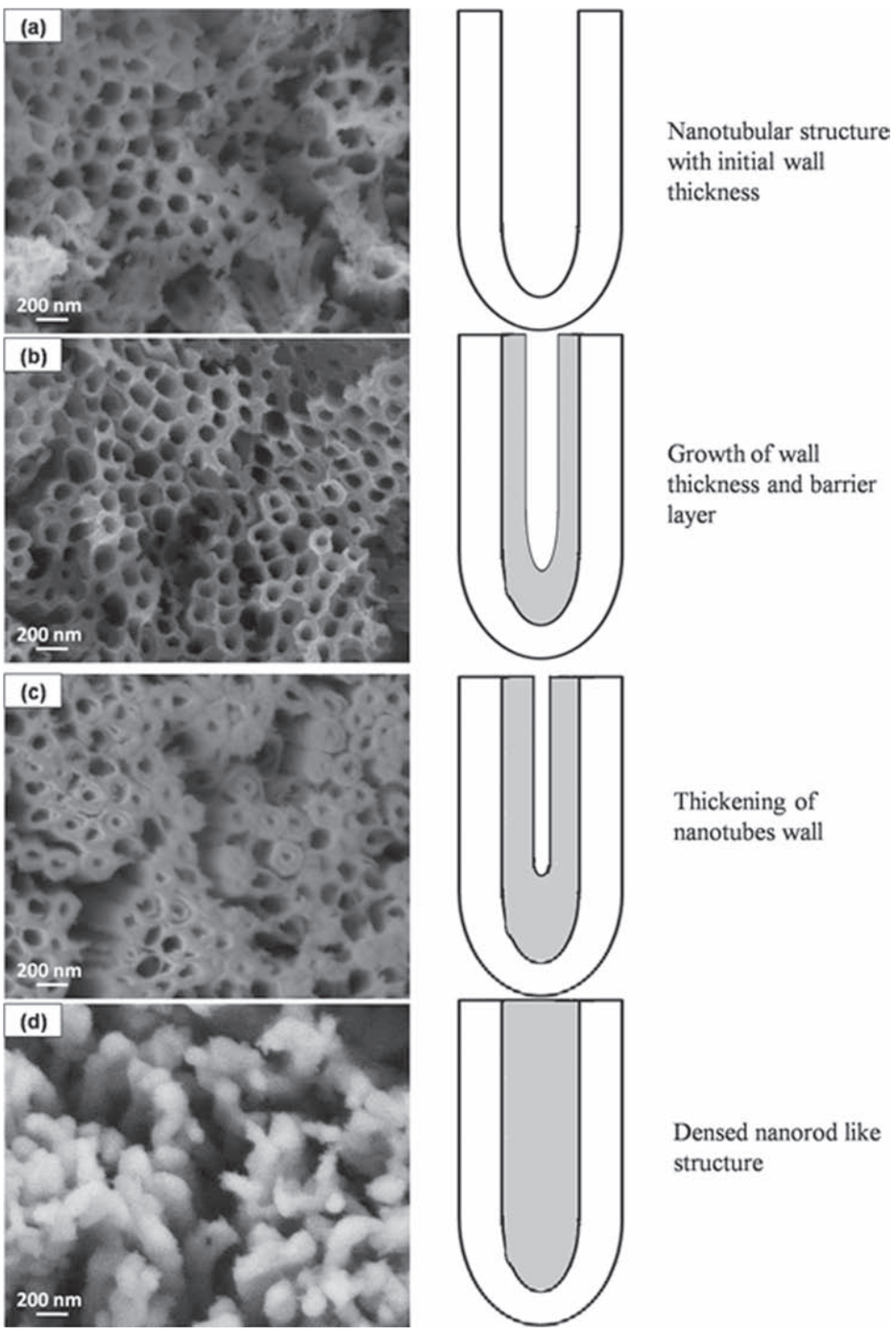

Fig. 8. FESEM images and schematic diagram of TiO_2 nanotube wall thickening of (a) as-anodized, and annealed at (b) 400 °C, (c) 500 °C, (d) 600 °C.

(284.9 eV).[37] The peak at 285.4 eV could be ascribed to Ti—C—O bonds that comprise the carbonate species. This happens when C atoms are incorporated into the interstitial positions of the TiO_2 lattice[41,42] during pyrogenation of the organic compound.[43]

Other than the information of TiO_2, binding energy of Al2p was traced at 72.1 eV, 72.2 eV and 73.9 eV. This is attributed to the binding energy of Al–O, which in agreement with that report by Li et al. 2009.[43] In addition, the $V2p_{3/2}$ peak corresponding to the metallic V appears at 515.5 eV and 518.2 eV. This is due to the fact that the affinity of Al and Ti with O is stronger than that of V. Al and Ti diffused outward, bringing on implanted layer outward growing, therefore V is deficient relatively in the outmost layer. However, the existing of oxidized state of Al, and the leaching of V contribute to reduce cellular toxicity of Al and V of Ti6Al4V as biomaterial.[43]

3.5. Crystal Structure of TiO_2 Nanotubes

Figure 7 shows the XRD pattern of the as-anodized and annealed TiO_2 nanotubes at different temperatures. Annealing is one of the most widely used post-fabrication procedures which increases crystallinity of as-produced amorphous TiO_2 nanotubes and removes surface fluorine to improve cell responses.[44] This result clearly shows that crystallization to the anatase structure occurs at low temperature (400 °C). This is the same finding as Ask et al. where they successfully induced crystallization to the anatase structure at temperatures in the range 300–400 °C.[45] Annealing at 400 °C has promoted the crystallization of anatase phase at 2θ of 25° and 48°, corresponding to (101) and (200) plane, respectively. At 500 °C, rutile peak (110) at 27.8° starts to exist. The weight fraction of anatase and rutile was 40% and 60% respectively. By increasing the temperature to 600 °C, the rutile peak with higher intensity is obtained, indicating the presence of rutile with a high degree of crystallinity. The weight fraction of anatase and rutile was 9% and 91% respectively.

The morphology schematic diagram of the as anodized TiO_2 nanotubes without heat treatment and annealed at 400 °C, 500 °C as well as 600 °C are shown in Figure 8. The morphology of the sample is significantly altered by the annealing process. Annealing at 400 °C ensured that the nanotube structure will not be changed (Fig. 8(b)). At 500 °C (Fig. 8(c)), thickening of TiO_2 nanotubes wall occurred due to mass transport involving Ti^{4+} diffusion at the bottom and wall of the TiO_2 nanotubes. Finally at 600 °C (Fig. 8(d)), tubular structure is completely damaged and nanorod like structure is formed. The change in morphology with annealing temperature is perhaps associated with the excessive diffusion of Ti ion along with the nanotube walls, which induced oxidation and thus thickened the oxide walls.

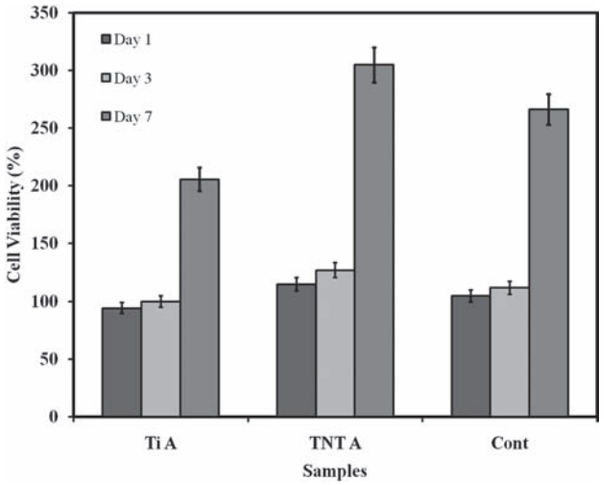

Fig. 9. MTS assay data showing the cell viability (%) of reaction product of the MTS working solution with PA6 cells cultured after 1, 3, 7 days of incubation. The error bars in the figure represent the standard deviation for four samples for each data. Ti A (Ti6Al4V alloy substrate), TNT A (TiO_2 nanotubes on Ti6Al4V alloy), Cont. (Control media).

3.6. Cell Attachment and Proliferation

To evaluate the viability of PA6 cells cultured on Ti6Al4V alloy, the MTS assays was employed in this study. After

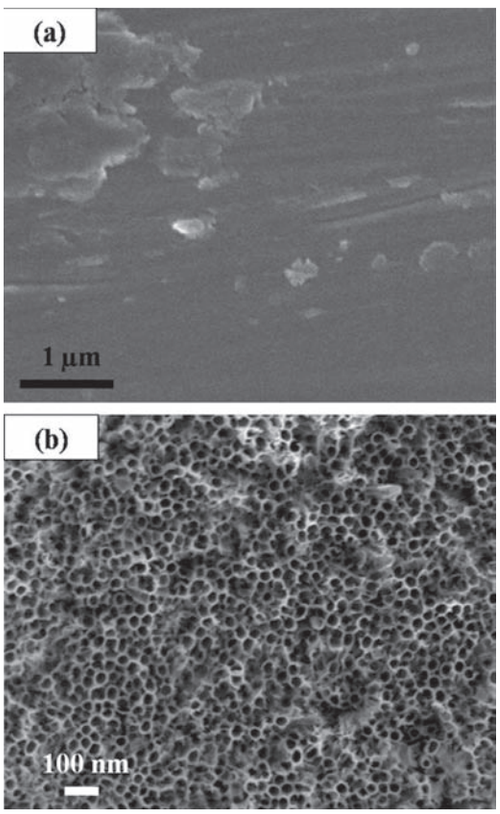

Fig. 10. FESEM images of (a) flat Ti6Al4V alloy substrate and (b) TiO_2 nanotubes layer on Ti6Al4V alloy.

RESEARCH ARTICLE

culturing for 1, 3 and 7 days, cell viability was quantified. The pale-yellow MTS assays are converted to purple formazon crystal only by the viable cells. Therefore the production of formazon indirectly reflects the viability of cells. As shown in Figure 9, after 7 days of culture, PA6s grown on anodized Ti6Al4V substrate showed statistically higher ($p < 0.001$) cell viability than those grown on flat Ti6Al4V alloy substrate. A similar trend was also found after 1 and 3 days of culture. It is well known those osteblast cells are likely to attach on rough surface layer.[46] Under FESEM (Fig. 10(a)) the Ti6Al4V alloy have rough contour surface morphology while TiO_2 nanotubes layer growth on Ti6Al4V alloy (Fig. 10(b)) was uniform. The adhesion of PA6 cell on day 7 was shown in Figure 11. Figure 11(a) shows that the PA6 cell on Ti6Al4V alloy substrate has filodopia like structure extending at the edge of the cell, while Figure 11(b) shows that almost every region of TiO_2 nanotubes surface have covered with PA6 cell. This result suggested that highly porous nanotubes structure on Ti6Al4V alloy promote the growth of PA6 bone marrow stromal cell lines consistently from day 1, 3 and 7 while the rough surface of Ti alloy substrate might induce stress to the cells and eventually arrest the cells proliferation cycle.[47] This indicates that PA6 cells may response differently to different surface structure. In addition, the surface energy and surface roughness of nanotubes would be essential factors for facilitating cells adhesion and proliferation.

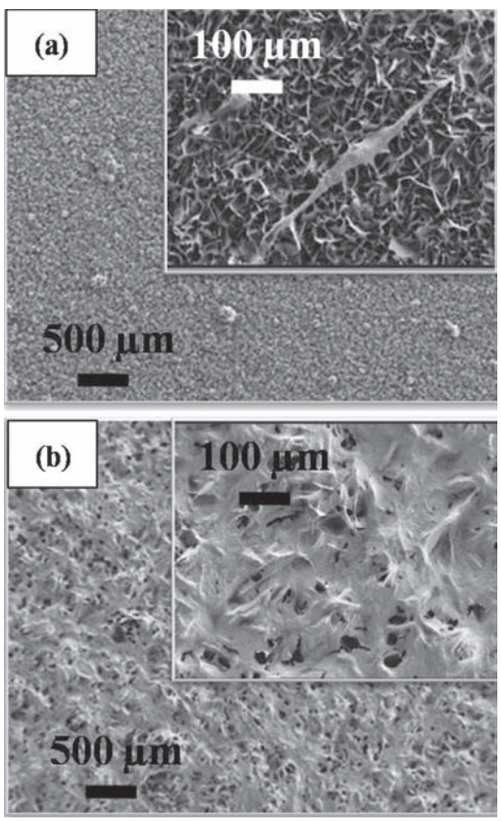

Fig. 11. FESEM images of PA6 bone marrow stromal cell cultured for 7 days on (a) flat Ti6Al4V alloy substrate and (b) TiO_2 nanotubes layer on Ti6Al4V alloy.

4. CONCLUSION

In this study, well aligned TiO_2 nanotube arrays on Ti6Al4V alloy were successfully developed. Under optimized voltage and fluoride content, the nanotubes length ranging from 1.6 μm to 9 μm were obtained after 6 hours anodization. Thermal annealing does influenced the crystallinity of TiO_2 nanotubes where transformation from amorphous to rutile phase has successfully occur at temperature 600 °C. It is found that the PA6 bone marrow stromal cells preferred to attach on TiO_2 nanotubes than flat Ti6Al4V alloy. Cells cultured on nanotubes showed highest level of viability and greater adhesion. Therefore, TiO_2 nanotubes provided a favorable surface structure for cell attachment and growth.

Acknowledgment: The authors would like to thank Universiti Sains Malaysia FRGS grant no. 6071213, and USM Fellowship for sponsoring this work. The authors gratefully acknowledge Straits Orthopaedics (Mfg) Sdn. Bhd. for providing the Ti6Al4V alloys.

References and Notes

1. M. Geetha, A. K. Singh, R. Asokamani, and A. K. Gogia, *Prog. Mater. Sci.* 54, 397 (**2009**).
2. P. Ducheyne and Q. Qiu, *Biomaterials.* 20, 2287 (**1999**).
3. E. Jallot, Encyclopedia of Nanoscience and Nanotechnology, edited by H. S. Nalwa, American Scientific Publishers, USA (**2004**), Vol. 7, p. 405.
4. S. Sreekantan, K. A. Saharudin, Z. Lockman, and T. W. Tzu, *Nanotechnology* 21, 365603 (**2010**).
5. S. Sreekantan, C. W. Lai, and Z. Lockman, *J. Electrochem. Soc.* 158, 397 (**2011**).
6. L. D. Sun, S. Zhang, X. W. Sun, and X. D. He, *J. Nanosci. Nanotechnol.* 10, 4551 (**2010**).
7. Z. Lockman, S. Ismail, G. Kawamura, and A. Matsuda, *Defect Diffus. Forum* 312, 76 (**2011**).
8. H. Jha, R. Hahn, and P. Schmuki, *Electrochim. Acta* 55, 8883 (**2010**).
9. A. Kaczmarek, T. Klekiel, and E. Krasicka-Cydzik, *Surf. Interface Anal*. 42, 510 (**2010**).
10. S. A. Catledge, M. Fries, and Y. K. Vohra, Encyclopedia of Nanoscience and Nanotechnology, edited by H. S. Nalwa, American Scientific Publishers, USA (**2004**), Vol. 7, p. 741.
11. H. Lukavoca , B. Plesingerova, M. Vojtko, and G. Ban, *Acta Metall. Slovac.* 16, 186 (**2010**).
12. B. Plesingerova, H. Lukavoca, D. Horkavcova, and M. Vojtko, *Acta Metall. Slovaca.* 14, 356 (**2008**).
13. S. Nishiguchi, H. Kato, H. Fujita, M. Oka, H.-M. Kim, T. Kokubo, and T. Nakamura, *Biomaterials* 22, 2525 (**2001**).
14. H. M. Kim, F. Miyaji, T. Kokubo, and T. Nakamura, *J. Biomed. Mater. Res.* 32, 409 (**1996**).
15. K. Maekawa, Y. Yoshida, A. Mine, T. Fujisawa, B. V. Meerbeek, K. Suzuki, and T. Kuboki, *J. Biomed. Mater. Res. A* 82, 195 (**2007**).
16. H. Tsuchiya, S. Berger, J. M. Macak, A. Ghicov, and P. Schmuki, *Electrochem. Commun.* 9, 2397 (**2007**).

RESEARCH ARTICLE

17. H. Tsuchiya, T. Akaki, J. Nakata, D. Terada, N. Tsuji, Y. Koizumi, Y. Minamino, P. Schmuki, and S. Fujimoto, *Corros. Sci.* 51, 1528 **(2009)**.

18. V. S. Saji, H. C, Choe, and W. A. Brantley, *Acta Biomater.* 5, 2303 **(2009)**.

19. A. Ghicov, S. Aldabergenova, H. Tsuchyia, and P. Schmuki, *Angew. Chem. Int. Ed.* 45, 6993 **(2006)**.

20. N. Aukland, A. Boudina, D. S. Eddy, J. V. Mantese, M. P. Thompson, and S. S. Wang, *J. Mater. Res.* 19, 1723 **(2004)**.

21. E. Matykina, J. M. Hernandez-Lopez, A. C. C. Domingo, J. J. de Damborenea, and M. A. Arenas, *Electrochim. Acta* 56, 2221 **(2011)**.

22. J. C. Keller, G. B. Schneider, C. M. Stanford, and B. Kellogg, *Implant Dent.* 12, 175 **(2003)**.

23. L. Marinucci, S. Balloni, E. Becchetti, S. Belcastro, M. Guerra, M. Calvitti, C. Lilli, E. M. Calvi, and P. Locci, *Int. J. Oral. Maxillofac. Implants.* 21, 719 **(2006)**.

24. S. Ozawa and S. Kasugai, *Biomaterials* 17, 23 **(1996)**.

25. M. Jayaraman, U. Meyer, M. Buhner, U. Joos, and H. P. Wiesmann, *Biomaterials* 25, 625 **(2004)**.

26. S. Guizzardi, C. Galli, D. Martini, S. Belletti, A. Tinti, M. Raspanti, P. Taddei, A. Ruggeri, and R. J. Scandroglio, *Periodontol.* 75, 273 **(2004)**.

27. B. Boyan, R. Batzer, K. Kieswetter, Y. Liu, D. L. Cochran, M. S. Szmuckler, D. D. Dean, and Z. Schwartz, *J. Biomed. Mater. Res.* 29, 77 **(1998)**.

28. K. Anselme, *Biomaterials* 21, 667 **(2000)**.

29. J. M. Macak., H. Hildebrand, U. Marten-Jahns, and P. Schmuki, *J. Electroanal. Chem.* 621, 254 **(2008)**.

30. C. W. Lai, S. Sreekantan, and Z. Lockman, *J. Nanosci. Nanotechnol.* 12, 4057 **(2012)**.

31. S. Sreekantan, K. A. Saharudin, and C. W. Lai, *IOP Conf. Ser.: Mater. Sci. Eng.* 21, 012002 **(2011)**.

32. L. Su, Y. X. Gan, and J. G. Lawrence, *Nanosci. Nanotechnol. Lett.* 4, 520 **(2012)**.

33. C. W. Lai and S. Sreekantan, *J. Nanomater.* 2011, 142463 **(2011)**.

34. B. Luo, H. Yang, S. Liu, W. Fu, P. Sun, M. Yuan, Y. Zhang, and Z. Liu, *Mater. Lett.* 62, 4512 **(2008)**.

35. S. K. Mohapatra, K. S. Raja, M. Misra, V. K. Mahajan, and M. Ahmadian, *Electrochim. Acta* 53, 590 **(2007)**.

36. J. Zhao, X. I. Wang, R. Chen, and L. Li, *Solid State Commun.* 134, 705 **(2005)**.

37. L. Y. Zi, D. S. Hwang, N. H. Lee, and S. J. Kim, *Chem. Phys. Lett.* 404, 25 **(2005)**.

38. J. Xie and B. L. Luan, *J. Mater. Res.* 23, 768 **(2008)**.

39. X. Hu, T. Zhang, Z. Jin, J. Zhang, W. Xu, J. Yan, J. Zhang, L. Zhang, and Y. Wu, *Mater. Lett.* 62, 4579 **(2008)**.

40. Y. Zhang, P. Xiao, X. Zhou, D. Liu, B. B. Garcia, and G. Cao, *J. Mater. Chem.* 19, 948 **(2009)**.

41. W. J. Ren, Z. H. Ai, F. L. Jia, L. Z. Zhang, X. X. Fan, and Z. G. Zou, *Appl. Catal. B* 69, 138 **(2007)**.

42. S. Sakthivel and H. Kisch, *Angew. Chem. Int. Edn.* 42, 4908 **(2003)**.

43. Y. Li, D. Y. Ding, C. Q. Ning, S. Bai, L. Huang, M. Li, and D. Mao, *Nanotechnology* 20, 065708 **(2009)**.

44. K. M. Kummer, E. Taylor, and T. J. Webster, *Nanosci. Nanotechnol. Lett.* 4, 483 **(2012)**.

45. M. Ask, U. Rolander, J. Lausmaa, and B. Kasemo, *Mater. Res.* 5, 1662 **(1990)**.

46. S. Oh, K. S. Brammer, K. S. Moon, J. M. Bae, and S. Jin, *Mater. Sci. Eng. C* 31, 873 **(2011)**.

47. G. M. de Peppo, A. Palmquist, P. Borchardt, M. Lenneras, J. Hyllner, A. Snis, J. Lausmaa, P. Thomsen, and C. Karlsson, *Scientific World Journal* 2012, 646417 **(2012)**.

Received: xx Xxxx xxxx. Accepted: xx Xxxx xxxx.

RESEARCH ARTICLE